DENTAL MATERIALS 35 (2019) 270–282

Available online at www.sciencedirect.com

ScienceDirect

journal homepage: www.intl.elsevierhealth.com/journals/dema

Effect of slow-cooling protocol on biaxial flexural strengths of bilayered porcelain-ceria-stabilized zirconia/alumina nanocomposite (Ce-TZP/A) disks

Tomofumi Sawada[a,b,*], *Verena Wagner*[a], *Christine Schille*[a], *Sebastian Spintzyk*[a], *Ernst Schweizer*[a], *Jürgen Geis-Gerstorfer*[a]

[a] *Section Medical Materials Science & Technology, University Hospital Tübingen, Osianderstr. 2-8, 72076 Tübingen, Germany*

[b] *Department of Biomedical Engineering, Iwate Medical University, 2-1-1 Nishitokuta, Yahaba-cho, Shiwa-gun, Iwate 028-3694, Japan*

ARTICLE INFO

Article history:
Received 20 June 2018
Received in revised form
13 November 2018
Accepted 15 November 2018

Keywords:
Ceria-stabilized zirconia/alumina nanocomposite (Ce-TZP/A)
Zirconia
Biaxial flexural strength
Veneering porcelain
Coefficient of thermal expansion (CTE)
Slow-cooling
Bilayered ceramic

ABSTRACT

Objective. The present study investigated the biaxial flexural strengths of bilayered ceria-stabilized zirconia/alumina nanocomposite (Ce-TZP/A) disks with various layering porcelains veneered using a slow-cooling protocol.

Methods. Five porcelain materials (VITA VM9, Cercon Ceram Kiss, and Vintage ZR with experimental coefficient of thermal expansions; CTEs of 8.45, 9.04, and 9.61 ppm/°C) were veneered on Ce-TZP/A disks and slow-cooled after firing to fabricate bilayered specimens (core-to-porcelain thickness: 0.8 mm/1.5 mm). Biaxial flexural strengths of the specimens with the porcelain layer in tension were tested based on the piston-on-three-ball method (ISO 6872:2008). The data were statistically analyzed using Weibull distribution and Fisher's exact test.

Results. Tensile stresses were observed in the entire porcelain layer while compressive stress at the surface of the Ce-TZP/A layer shifted to tensile stress at the interface between the materials. The cases of small CTE mismatches between the materials showed high Weibull characteristic strengths at the internal and external surfaces of the specimens, except the VM9 group (CTE: 9.0–9.2 ppm/°C). The maximum tensile stress was observed on the surface of the porcelain layer, where cracks originated and continuously propagated into the Ce-TZP layer. The Ce-TZP/A fractured into two pieces for large CTE mismatches between the materials, resulting in significantly lower flexural strengths than those fracturing into three pieces for small CTE mismatches.

Significance. Flexural strengths and fracture behaviors of bilayered porcelain-Ce-TZP/A disks were influenced by the CTE mismatches, and a small CTE mismatch between the materials was preferred when using a slow-cooling protocol.

* *Corresponding author.*
E-mail addresses: sawada@iwate-med.ac.jp, Tomofumi.Sawada@med-uni-tuebingen.de (T. Sawada), verena.wagner@student.uni-tuebingen.de (V. Wagner), christine.schille@med.uni-tuebingen.de (C. Schille), Sebastian.Spintzyk@med.uni-tuebingen.de (S. Spintzyk), ernst.schweizer@med.uni-tuebingen.de (E. Schweizer), geis-gerstorfer@mwt-tuebingen.de (J. Geis-Gerstorfer).

https://doi.org/10.1016/j.dental.2018.11.024

1. Introduction

All-ceramic dental restorations require good esthetic appearance and sufficient mechanical properties to withstand occlusal or chewing forces because of the inherent brittleness of ceramic systems, which leads to premature failure by repeated contact loading in moist environments [1]. In zirconia-based prosthodontic restorations, ceria-stabilized zirconia/alumina (Ce-TZP/A) nanocomposite ceramic is a promising alternative due to its superior characteristics of high fracture toughness, absence of low-temperature degradation, and reduced framework thickness relative to conventional yttria-stabilized tetragonal zirconia polycrystals (Y-TZP) [2–6]. These advantageous properties allow effective application of Ce-TZP/A in short-span (3 or 4 units) and long-span (up to full-arch) fixed partial dentures (FPDs). However, it must be layered with the veneering porcelain for esthetic reasons due to its dull white color and low light transmittance [7,8].

Fractures of the veneering porcelain, such as cohesive failures within the porcelain layer (chipping) or adhesive failures between the porcelain-zirconia interface (delamination) under functional loading, seriously impact the outcomes of bilayered restorations [9,10]. In fact, Y-TZP-based FPDs show lower survival rates with higher frequencies of porcelain chipping and loss of retention than metal-ceramic FPDs [11,12]. Even though Y-TZP-based posterior FPDs showed similar survival rates as metal-ceramic FPDs in a recent clinical trial, large fractures of the porcelain and debonding were only observed in Y-TZP-based restorations [13]. In contrast, clinical evidences of Ce-TZP-based restorations are for relatively short periods (up to 3 years) and quite less published, showing acceptable short-term survival rates [14–16]. However, one study reported that Ce-TZP/A frameworks allowed excellent marginal adaptation, but were susceptible to veneering failures [16].

For achieving long-term clinical success, the compatibility between the porcelain and zirconia framework is crucial in bilayered ceramic systems. The differences in the coefficient of thermal expansion (CTE) and phase changes during cooling after porcelain firing lead to thermal mismatches between materials, resulting in transient or residual stresses within restorations [17–19]. The mechanism of porcelain-zirconia interface adhesion is yet to be ascertained and the exact range of thermal compatibility is unclear for bilayered zirconia-based restorations [20,21]. However, porcelains seem to be mainly bonded to zirconia with mechanical interlocking and compressive stress due to small differences between materials resulting in thermal shrinkage by cooling [7]. In previous studies [10,22], the surface treatment of the Y-TZP substrate improved the porcelain-Y-TZP bond strength and fracture strength, depending on the particle size of the sandblasting. Furthermore, a slight compressive stress in the porcelain layer is favorable for enhancing the reinforcement of porcelain and fracture strengths of Y-TZP-based crowns for bilayered systems [17]. Hence, commercial products of porcelain are generally designed to have slightly lower CTE values than that of Y-TZP [7].

Meanwhile, for Ce-TZP/A-based restoration, whether various commercial porcelains for Y-TZP should be applied to frameworks for clinical use is still under question as Ce-TZP/A has a lower CTE value (10.3 ppm/°C) than Y-TZP (approximately 10.5 ppm/°C) [18]. Some researchers have reported the compatibility between porcelain and Ce-TZP/A framework using different testing methodologies *in vitro* [18,23,24]. Fischer and Stawarczyk [18] showed that the fracture strength of bilayered specimens in Ce-TZP/A was equal or lower than that in Y-TZP as the CTE of Ce-TZP/A is closer to that of the porcelain. Therefore, the authors suggested that a veneering ceramic with an appropriate coefficient of thermal expansion has to be designed for Ce-TZP/A because it has inferior compatibility with commercial porcelain compared to Y-TZP.

To identify the optimum porcelain material for Ce-TZP/A, we recently examined biaxial flexural strengths in bilayered porcelain-Ce-TZP/A disks prepared using commercial and experimental porcelains with various layer thicknesses and using a conventional normal-cooling (fast-cooling) protocol [25]. We verified that the internal and external stresses in the bilayered disk were influenced by the porcelain thickness and CTE. Since the maximum tensile stress was located at the interface for the thin porcelain layer (1.0 mm), optimum behavior was observed for combinations with a small CTE mismatch between the materials and low core-to-porcelain thickness ratio. However, there is limited information on this because multiple factors, such as mechanical properties of substrate materials, characteristics of porcelain, and manufacturing processes of restorations, influence the strengths of zirconia-based restorations [26–28]. In previous research of Y-TZP, due to differences in thermal diffusivities and conductivities between materials, the cooling protocol after firing influenced the longevity of bilayered restorations and depended on the cooling rate, porcelain layer thickness, and CTE mismatch [29–31]. For instance, a slow-cooling protocol increased the resistance and lifetime of Y-TZP-based crowns even though porcelain that showed larger a thermal mismatch with Y-TZP was used [29].

Thus, we hypothesize that bilayered porcelain-Ce-TZP/A disks improve compatibility due to larger a CTE mismatch with porcelain compared with Y-TZP, when a slow-cooling protocol is applied. The aim of this study was to evaluate biaxial flexural strengths of bilayered Ce-TZP/A-based disks using various porcelain materials with a slow-cooling protocol. The null hypothesis was that biaxial flexural strengths and fracture behaviors on bilayered porcelain-Ce-TZP/A disks were not changed by the porcelain materials. Based on previous studies, the calculation of biaxial flexural strengths for bilayered disks was performed using recent closed-form solutions derived by Hsueh et al. and Hsueh and Kelly [25,32–34]. Prior to biaxial flexural testing, due to the CTE mismatch resulting in thermal stress gradient in each layer of bilayered disks, thermal stress distributions were also evaluated using other closed-form solutions derived by Hsueh et al. [35,36].

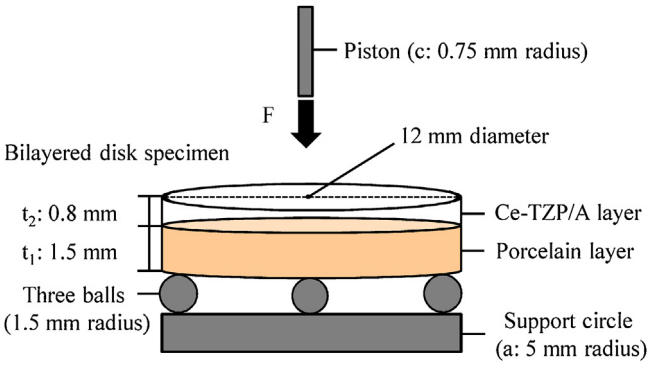

Fig. 1 – A schematic of the piston-on-three-ball biaxial flexural test.

2. Materials and methods

2.1. *Preparation of bilayered porcelain-Ce-TZP/A specimens*

Ce-TZP/A disks (12 mm diameter × 0.8 mm thickness; C-Pro Nano-Zirconia, Panasonic Healthcare, Tokyo, Japan), two commercial porcelains (VM9: VITA VM9, VITA Zahnfabrik, Bad Säckingen, Germany, and CCK: Cercon Ceram Kiss, Degudent, Hanau-Wolfgang, Germany), and one experimental porcelain (Vintage ZR, Shofu Inc., Kyoto, Japan) with three different CTE values (8.45, 9.04, and 9.61 ppm/°C, respectively), were used (Table 1). The porcelain material was applied to the Ce-TZP/A disk and fired in a dental furnace (Austromat 654 press-i-dent, Dekema Dental-Keramiköfen, Freilassing, Germany) (Table 2). The layering procedure was comprised of four steps as follows: the application of an opaque liner, then the first and second dentin, followed by glazing. Each porcelain powder was mixed with a respective liquid, and the mixture slurry was applied on the disk using a thin brush. Excess moisture was removed by tissue paper during the application. Slow-cooling was performed by the modified protocol based on a previous report in which the firing chamber was closed until the temperature reached 50 °C below the glass transition temperature (T_g) of porcelain [37]; the moving stage was partially set down by maintaining with the temperature at 65% of the firing temperature (5 min; extended cooling time), and then completely set down when the temperature decreased to the basic temperature. The specimens were then taken out of the furnace and cooled to room temperature. During dentin application, a special holder was used to fabricate the accurate porcelain layer thickness (1.5 mm) on the disk. Finally, the dimension of each bilayered specimen (12 mm diameter × 2.3 mm thickness, Fig. 1) was verified using an electronic digital caliper ($n = 10$ per group).

2.2. *Analysis of thermal stress distribution*

For bilayered dental ceramics, combined tension/compression stresses by thermal stress gradient that occur in the respective layer depend on the layer thickness and mechanical property [36]. Thus, biaxial thermal stress distributions through the entire layer thicknesses of the specimens were evaluated using the following formulas derived by Hsueh et al. [35,36]:

$$\sigma_1 = E_1'\{\frac{E_2' t_2(\alpha_2-\alpha_1)\Delta T}{E_1' t_1 + E_2' t_2} + k[z - \frac{E_1' t_1^2 + E_2' t_2^2 + 2E_2' t_1 t_2}{2(E_1' t_1 + E_2' t_2)}]\} \times \quad (\text{for} \quad 0 \le z \le t_1), \tag{1}$$

$$\sigma_2 = E_2'\{\frac{E_1' t_1(\alpha_1-\alpha_2)\Delta T}{E_1' t_1 + E_2' t_2} + k[z - \frac{E_1' t_1^2 + E_2' t_2^2 + 2E_2' t_1 t_2}{2(E_1' t_1 + E_2' t_2)}]\} \times \quad (\text{for} t_1 \le z \le t_1 + t_2), \tag{2}$$

$$E' = \frac{E}{1-\nu}, \tag{3}$$

$$k = \frac{6E_1' E_2' t_1 t_2 (t_1+t_2)(\alpha_2-\alpha_1)\Delta T}{E_1'^2 t_1^4 + E_2'^2 t_2^4 + 2E_1' E_2' t_1 t_2 (2t_1^2 + 2t_2^2 + 3t_1 t_2)}, \tag{4}$$

where subscript 1 refers to the porcelain layer and subscript 2 refers to the Ce-TZP/A layer in all cases, σ is the thermal stress, E is the elastic modulus, z is the vertical cylindrical coordinate, ν is the Poisson's ratio, t is the layer thickness (mm), α is the CTE value, ΔT is the temperature change from the stress-free temperature, and k is the curvature of the bilayer (Table 1, Fig. 1).

2.3. *Biaxial flexural tests*

Flexural strengths were evaluated based on the biaxial flexural test according to ISO 6872:2008 (piston-on-three-ball method) [38]. The specimen was fixed on three balls (with a diameter of 3.0 mm) which were placed 120° apart on a support circle (with a diameter of 10 mm) using a special device (Fig. 1). The test was conducted using a universal testing machine (Z010, Zwick, Ulm, Germany) at a 1.0 mm/min crosshead speed until fracture. Load was applied to the center of the Ce-TZP/A surface using a flat piston. The fracture load (P) was then recorded.

First, the biaxial flexural strengths in the porcelain (σ_1) and Ce-TZP/A (σ_2) layers of the specimen were calculated using the following formulas derived by Hsueh et al. [32]:

$$\sigma_1 = \frac{-E_1(z-z^*)P}{8\pi(1-\nu_1)D^*}\{1 + 2\ln(\frac{a}{c}) + \frac{1-\nu_{ave}}{1+\nu_{ave}}[1 - \frac{c^2}{2a^2}]\frac{a^2}{R^2}\} \times \quad (\text{for} \quad 0 \le z \le t_1 \quad \text{and} \quad r \le c), \tag{5}$$

$$\sigma_2 = \frac{-E_2(z-z^*)P}{8\pi(1-\nu_2)D^*}\{1 + 2\ln(\frac{a}{c}) + \frac{1-\nu_{ave}}{1+\nu_{ave}}[1 - \frac{c^2}{2a^2}]\frac{a^2}{R^2}\} \times \quad (\text{for} \quad t_1 \le z \le t_1 + t_2 \quad \text{and} \quad r \le c), \tag{6}$$

$$z^* = \frac{E_1 t_1^2/2(1-\nu_1^2) + E_2 t_2^2/2(1-\nu_2^2) + E_2 t_1 t_2/(1-\nu_2^2)}{E_1 t_1/(1-\nu_1^2) + E_2 t_2/(1-\nu_2^2)}, \tag{7}$$

Table 1 – Materials used in this study.

Material	Product name (code)	Manufacture	CTE, α (ppm/°C)	E-modulus (GPa)	Poisson's ratio	T_g (°C)
Ce-TZP/A	C-Pro Nano-Zirconia	Panasonic Healthcare	10.3[a]	245[a]	0.29[a]	–
Commercial porcelain	VITA VM9 (VM9)	VITA Zahnfabrik	9.1:9.0–9.2[a]	64.57[a]	0.21[a]	600[a]
	Cercon ceram Kiss (CCK)	DeguDent	9.2[a]	75[a]	0.20[a]	575[a]
Experimental porcelain	Vintage ZR (Experimental 8.45, 9.04, 9.61)	Shofu	8.45, 9.04, 9.61	66.4[a]	0.22[a]	605

CTE: coefficient of thermal expansion, T_g: glass transition temperature, Ce-TZP/A: ceria-stabilized zirconia/alumina nanocomposite.
[a] As disclosed by manufactures when obtaining the materials.

Table 2 – Firing schedules of veneering porcelains.

Porcelain (CTE; ppm/°C)	Procedure	Basic (°C)	Dry (min)	Temperature increase (°C/min)	Firing (°C)	Hold (min)	Extended cooling (min)	Vacuum (%)
VM9	Liner	500	6	55	930	1	–	100
(9.1:9.0–9.2)	Dentin (1st)	500	6	55	910	1	–	100
	Dentin (2nd)	500	6	55	900	1	–	100
	Glaze	500	4	80	870	1	5	–
CCK	Liner	500	6	55	930	1	–	100
(9.2)	Dentin (1st)	450	5	55	830	1	–	100
	Dentin (2nd)	450	5	55	820	1	–	100
	Glaze	450	3	55	800	1	5	–
Experimental	Liner	500	8	45	930	1	–	100
(8.45, 9.04, and 9.61)	Dentin (1st)	650	6	45	910	1	–	100
	Dentin (2nd)	650	6	45	900	1	–	100
	Glaze	600	6	55	860	1	5	–

VM9: VITA VM 9, CCK: Cercon Ceram Kiss, Experimental: Vintage ZR.

$$D^* = \frac{E_1 t_1^3}{3(1-\upsilon_1^2)} + \frac{E_2 t_2^3}{3(1-\upsilon_2^2)} + \frac{E_2 t_1 t_2 (t_1+t_2)}{(1-\upsilon_2^2)} - \frac{\left[E_1 t_1^2/2(1-\upsilon_1^2) + E_2 t_2^2/2(1-\upsilon_2^2) + E_2 t_1 t_2/(1-\upsilon_2^2)\right]^2}{E_1 t_1/(1-\upsilon_1^2) + E_2 t_2/(1-\upsilon_2^2)}, \quad (8)$$

$$\upsilon_{ave} = \frac{\upsilon_1 t_1 + \upsilon_2 t_2}{t_1 + t_2}, \quad (9)$$

where a is the radius of the support circle (5 mm), c is the radius of the loading piston (0.75 mm), R is the radius of the specimen (mm), z^* is the neutral surface position, D^* is the flexural rigidity, and ν_{ave} is the average Poisson's ratio (Fig. 1).

Second, the biaxial stresses at the top (σ_T) and bottom (σ_B) surfaces of the specimen were calculated using the following formulas derived by Hsueh and Kelly [33]:

$$\sigma_T = \frac{(6E_2M/(1-\nu_2)[E_1t_1^2/((1-\nu_1) + E_2t_2^2/(1-\nu_2) + 2E_1t_1t_2/(1-\nu_1)]}{[E_1t_1^2/(1-\nu_1) + E_2t_2^2/(1-\nu_2)]^2 + 4E_1E_2t_1t_2(t_1^2 + t_1t_2 + t_2^2)/((1-\nu_1)(1-\nu_2))}, \quad (10)$$

$$\sigma_B = \frac{(-6E_1M/(1-\nu_1)[E_1t_1^2/((1-\nu_1) + E_2t_2^2/(1-\nu_2) + 2E_2t_1t_2/(1-\nu_2)]}{[E_1t_1^2/(1-\nu_1) + E_2t_2^2/(1-\nu_2)]^2 + 4E_1E_2t_1t_2(t_1^2 + t_1t_2 + t_2^2)/((1-\nu_1)(1-\nu_2))}, \quad (11)$$

$$M = \frac{-P}{8\pi}\{(1+\nu_{ave})[1 + 2\ln(\frac{a}{c}) + (1-\nu_{ave})[(1 - \frac{c^2}{2a^2})\frac{a^2}{R^2}]\} \times \quad (\text{for } r \le c), \quad (12)$$

where M is the biaxial moment.

Additionally, the stresses at the interface between the bottom (σ_1) and top (σ_2) layers of the specimen were calculated as follows:

$$\sigma_1 = \frac{E_1(1-\upsilon_2)t_1\sigma_T}{E_2(1-\nu_1)(t_1+t_2)} + \frac{t_2\sigma_B}{t_1+t_2} \quad (at\ z = t_1), \quad (13)$$

$$\sigma_2 = \frac{t_1\sigma_T}{t_1+t_2} + \frac{E_2(1-\nu_1)t_2\sigma_B}{E_1(1-\nu_2)(t_1+t_2)} \quad (at\ z = t_1), \quad (14)$$

After testing, the fractured specimens were observed using stereomicroscopy (Wild Heerbrugg, Heerbrugg, Switzerland) and scanning electron microscopy (SEM; LEO 1430, Carl Zeiss, Oberkochen, Germany).

2.4. *Data analysis*

The calculated biaxial flexural strengths were evaluated using the Weibull characteristic strength and modulus according to ISO 6872:2008, because ceramic strength data is inhomogeneous and distributed over the high-strength region [38,39]. Thus, the variability of the flexural strength values was ana-

Table 3 – Distributions of biaxial thermal stresses (σ; MPa).

Porcelain material	Thermal stress (σ; MPa)			
(CTE; ppm/°C)	σ_2[a] ($z=t_1+t_2$)	σ_2 ($z=t_1$)	σ_1[a] ($z=t_1$)	σ_1 ($z=0$)
VM 9 (9.1:9.0–9.2)	43.6	80.4	37.4	17.7
CCK (9.2)	36.8	72.1	37.1	18.3
Experimental (8.45)	67.5	126.6	60.6	29.1
Experimental (9.04)	46.0	86.2	41.3	19.8
Experimental (9.61)	25.2	47.3	22.6	10.9

CTE: coefficient of thermal expansions, σ_1, σ_2: thermal stresses at the bottom (porcelain) and top (Ce-TZP/A) layers of the specimen, respectively. VM9: VITA VM 9, CCK: Cercon Ceram Kiss, Experimental: Vintage ZR.
[a] Indicates the compressive stress.

lyzed using the two-parameter Weibull distribution function [40]. The Weibull distribution is given by the following formula: $P_f = 1 - \exp[-(\sigma/\sigma_0)^m]$, where P_f is the probability of failure, σ is the flexural strength in MPa, σ_0 is the Weibull characteristic strength (σ_0) when the failure probability is 63.2%, and m is the Weibull modulus (m) describing the shape of the strength distribution as a function of failure probability. The values of σ_0 and m, and 95% confidence intervals (CI) were computed using the maximum likelihood estimation method [41]. The parameters were analyzed by chi-square tests with the Bonferroni simultaneous 95% CI. In addition, the number of fracture fragments of the Ce-TZP/A substrate was compared using Fisher's exact test. Statistical analyses were performed using Minitab version 18 (Minitab Inc., State College, PA, USA) and R version 3.2.3 (The R Foundation for Statistical Computing, Vienna, Austria). A p-value of 0.05 was considered statistically significant.

3. Results

3.1. Thermal stresses

Thermal stress distributions through the entire layer thicknesses of the specimens are shown in Fig. 2a. Irrespective of the porcelain material, the surface of the Ce-TZP/A layer (σ_2; $z=t_1+t_2$) indicated compressive stresses shifted to tensile stresses at the interface between the materials (σ_2; $z=t_1$) while the interface (σ_1; $z=t_1$) indicated tensile stresses shifted to compressive stresses at the surface of the porcelain layer (σ_1; $z=0$) (Table 3). Thus, biaxial thermal stresses were discontinuous at the interfaces of the layers, and their stress gradients differed. For commercial porcelain (VM9 and CCK), the magnitudes of stresses and the stress gradients showed similar behavior. In contrast, for experimental porcelain groups, the magnitudes of these stresses were higher when using porcelain with lower CTE, resulting in large stress differences at the interface between materials.

3.2. Biaxial flexural strengths

Using the formulas for the respective layers (Eqs. (5)–(9)), the calculated σ_1 values indicated tensile stresses in the porcelain layer while the σ_2 values showed compressive stresses in the Ce-TZP/A layer (Table 4). In the porcelain layer (σ_1), the specimens using the experimental porcelain with CTEs of 9.04 and 9.61 ppm/°C showed significantly higher characteristic strengths than those using CCK and the experimental porcelain with a CTE of 8.45 ppm/°C ($p<0.001$). Moreover, VM9 showed significantly higher strength than CCK between the commercial porcelains ($p<0.001$). In the Ce-TZP/A layer (σ_2), an additional significant difference was observed between VM9 and the experimental porcelain with a CTE of 9.04 ppm/°C ($p<0.001$). The VM9 specimens showed significantly higher m values than the specimen using the experimental porcelain with a CTE of 9.61 ppm/°C ($p<0.001$).

From the formulas for the surfaces of the respective layers (Eqs. (10)–(12)), the σ_T and σ_B values showed compressive and tensile stresses at the top and bottom surfaces of the specimens, respectively (Fig. 2b, Table 5). The significant differences in Weibull characteristic strengths and moduli of σ_T and σ_B using the Hsueh and Kelly formulas are the same as those of σ_1 and σ_2 as calculated using the Hsueh et al. formulas.

Furthermore, from the formulas for the interfaces of the specimens (Eqs. (13) and (14)), the results of σ_1 (Ce-TZP/A side) and σ_2 (porcelain side) showed tensile stresses. The CCK specimens showed the lowest strengths ($p<0.001$), except for the experimental porcelain with a CTE of 8.45 ppm/°C. The significant differences in m values had a similar trend as the other parameters.

At the interfaces of the specimens, the σ_2 values showed higher strengths than the σ_1 values, irrespective of the porcelain material (Fig. 2b). Between commercial porcelains, the difference ($\Delta\sigma_2 - \sigma_1$) in VM9 specimens was higher than that in CCK specimens. Meanwhile, these differences increased with increasing in CTE values amongst experimental porcelains. Further, the σ_B values were higher than σ_2 in all specimens. The difference ($\Delta\sigma_B - \sigma_2$) in CCK specimens was slightly higher than in VM9 specimens between commercial porcelains while the difference ($\Delta\sigma_B - \sigma_2$) increasing with increase in CTE values among the experimental porcelains.

3.3. Fracture behavior after testing

The Ce-TZP/A substrates were completely fractured in all the specimens after testing. However, the number of fracture fragments from the Ce-TZP/A depended on the porcelain material (Fig. 3, Table 6). The Ce-TZP/A fractured into two pieces were significantly higher in VM9, CCK, and the experimental porcelain with a CTE of 8.45 ppm/°C, while those fractured into three pieces were dominant for the experimental porcelain with a CTE of 9.61 ppm/°C ($p=0.016$). Additionally, the Mann–Whitney U test proved that all the parameters of Weibull characteristic strength were significantly higher in the specimens with three pieces of Ce-TZP/A fracture than those with two pieces ($p<0.05$, Fig. A1).

Fractures in the specimens always originated at the bottom surface of the porcelain layer and crack propagations were continuous toward the interface and then through the Ce-TZP layer (Fig. 3). In particular, a semicircular defect in the Ce-TZP/A substrate at the interface was clearly observed in the specimens with two fractured pieces of Ce-TZP/A (Fig. 3c) while only fracture lines in the Ce-TZP/A layer were observed in those with three fractured pieces (Fig. 3d).

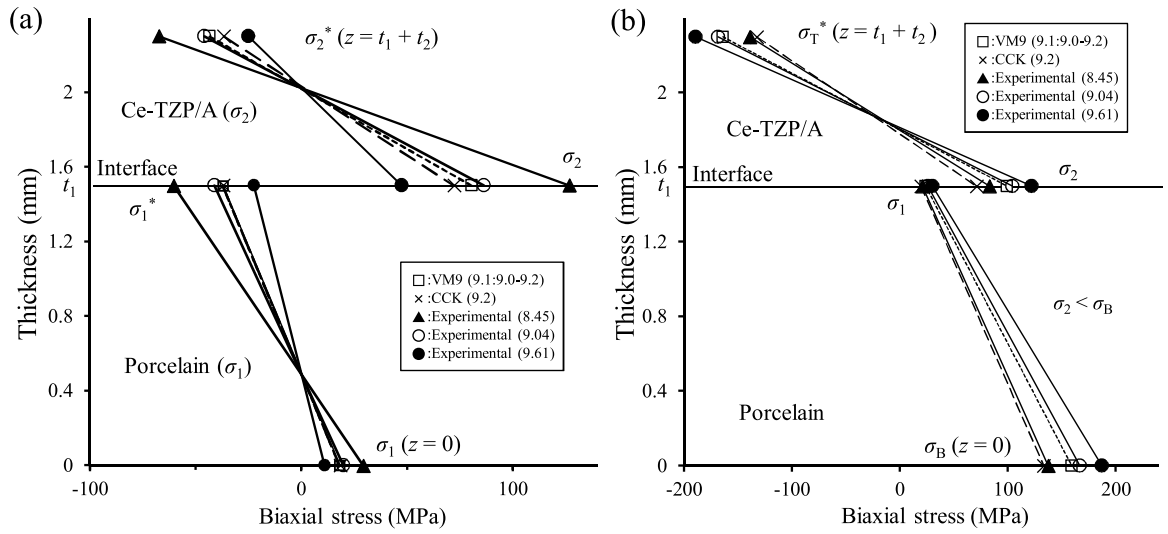

Fig. 2 – Stress distributions through the entire thickness of bilayered specimens (a) biaxial thermal stress, and (b) biaxial stress subjected to piston-on-three-ball tests. VM9: VITA VM 9, CCK; Cercon Ceram Kiss, Experimental porcelain: Vintage ZR (CTE: ppm/°C). * indicates the compressive stress.

Table 4 – Comparison of biaxial flexural strengths (σ; MPa) calculated using the Hsueh et al. formulas, Weibull characteristic strength (σ_0; MPa) and modulus (m) for each group.

Porcelain material	BFS (σ; MPa)	Characteristic strength (MPa)	Weibull modulus
(CTE; ppm/°C)	Mean (SD)	σ_0 (95% CI)	m (95% CI)
σ_2[1] ($z = t_1 + t_2$)		($p < 0.001$)	($p < 0.001$)
VM 9 (9.1:9.0–9.2)	324.1 (21.6)	333.5^{a} (321.8–345.6)	18.4^{a} (11.3–29.8)
CCK (9.2)	256.1 (40.5)	270.6^{b} (253.5–288.8)	9.9^{ab} (5.8–16.7)
Experimental (8.45)	264.5 (41.9)	281.8^{b} (255.9–310.4)	6.8^{ab} (4.4–10.6)
Experimental (9.04)	324.7 (38.3)	341.5^{a} (317.8–366.9)	9.2^{ab} (5.8–14.5)
Experimental (9.61)	351.2 (82.1)	383.4^{a} (327.0–449.5)	4.2^{b} (2.7–6.3)
σ_1 ($z = 0$)		($p < 0.001$)	($p < 0.001$)
VM 9 (9.1:9.0–9.2)	154.5 (10.3)	159.0^{ac} (153.4–164.8)	18.3^{a} (11.3–29.8)
CCK (9.2)	131.1 (20.8)	139.1^{b} (130.3–148.5)	9.8^{ab} (5.8–16.7)
Experimental (8.45)	127.5 (20.4)	135.9^{ab} (123.3–149.8)	6.7^{ab} (4.3–10.6)
Experimental (9.04)	156.7 (18.5)	164.8^{c} (153.3–177.1)	9.1^{ab} (5.8–14.5)
Experimental (9.61)	169.5 (39.7)	185.0^{c} (157.8–217.0)	4.2^{b} (2.7–6.3)

CTE: coefficient of thermal expansions, BFS: biaxial flexural strength, σ_1, σ_2: biaxial flexural strengths at the bottom and top layers of the specimen, respectively. VM9: VITA VM 9, CCK: Cercon Ceram Kiss, Experimental: Vintage ZR. Different lowercase letters within each parameter indicate significant differences among the groups ($p < 0.05$).
[1] Indicates the compressive stress.

4. Discussion

Dental professionals still find it difficult to select porcelain material for Ce-TZP/A-based restorations because Ce-TZP/A has a different chemical composition, crystal structure, and CTE value than Y-TZP. Evidence concerning the biaxial flexural strength for a Ce-TZP/A-based system is still not adequate. We first demonstrated that bilayered porcelain-Ce-TZP/A disks prepared using a fast- (normal-) cooling protocol affected biaxial flexural strengths depending on CTE mismatches between the materials and porcelain layer thickness [25]. In consideration of multiple factors, the biaxial flexural tests performed here were conducted for porcelain-Ce-TZP/A disks prepared using a slow-cooling protocol, and porcelain materials affected biaxial flexural strengths and fracture behaviors of the disks, thus rejecting the null hypothesis.

4.1. *Calculated thermal stresses*

First, the residual thermal stresses in the bilayered structure during cooling may influence the longevity of the restorations. Porcelain generally cools from the outer to the inner surface, and residual stresses develop in Y-TZP-based restorations [42–44]. The biaxial thermal stress distributions observed here resulted in high-magnitude stresses in most specimens using lower CTE porcelain due to large thermal (CTE) mismatches between the materials (Fig. 2a). Accordingly, the experimental porcelain with a CTE of 9.61 ppm/°C might be a better choice for the Ce-TZP/A substrate in our cases, which resulted in slight residual compressive stresses (−22.6 MPa) at the inter-

Table 5 – Comparison of biaxial flexural strengths (σ; MPa) calculated using Hsueh and Kelly formulas, Weibull characteristic strength (σ_0; MPa) and modulus (m) for each group.

Porcelain material	BFS (σ; MPa)	Characteristic strength (MPa)	Weibull modulus
(CTE; ppm/°C)	Mean (SD)	σ_0 (95% CI)	m (95% CI)
σ_T[1] (Ce-TZP/A surface)		($p < 0.001$)	($p < 0.001$)
VM 9 (9.1:9.0–9.2)	159.7 (10.6)	164.4^{a} (158.6–170.4)	18.3^{a} (11.3–29.7)
CCK (9.2)	125.8 (19.9)	132.9^{b} (124.5–141.9)	9.9^{ab} (5.8–16.7)
Experimental (8.45)	130.7 (20.8)	139.3^{b} (126.4–153.5)	6.8^{ab} (4.3–10.6)
Experimental (9.04)	160.6 (19.0)	168.9^{a} (157.1–181.5)	9.1^{ab} (5.8–14.5)
Experimental (9.61)	173.7 (40.8)	189.7^{a} (161.7–222.5)	4.1^{b} (2.7–6.3)
σ_2 (Ce-TZP/A interface)		($p < 0.001$)	($p < 0.001$)
VM 9 (9.1:9.0–9.2)	94.9 (9.2)	99.0^{a} (93.3–105.0)	11.2^{a} (7.1–17.6)
CCK (9.2)	66.3 (11.5)	70.6^{b} (65.3–76.3)	8.3^{ab} (4.9-14.0)
Experimental (8.45)	75.4 (19.4)	82.5^{ab} (71.2–95.5)	4.5^{ab} (2.8–7.1)
Experimental (9.04)	97.5 (15.1)	104.0^{a} (94.2–114.8)	6.7^{a} (4.3–10.4)
Experimental (9.61)	109.4 (36.1)	121.7^{a} (98.1–151.1)	3.1^{b} (2.0–4.6)
σ_1(Porcelain interface)		($p < 0.001$)	($p < 0.001$)
VM 9 (9.1:9.0–9.2)	22.5 (2.2)	23.4^{a} (22.1–24.9)	11.2^{a} (7.1–17.6)
CCK (9.2)	18.0 (3.1)	19.2^{b} (17.7–20.7)	8.3^{ab} (4.9–14.0)
Experimental (8.45)	18.6 (4.8)	20.4^{ab} (17.6–23.6)	4.5^{ab} (2.8–7.1)
Experimental (9.04)	24.1 (3.7)	25.6^{a} (23.2–28.3)	6.7^{ab} (4.3–10.4)
Experimental (9.61)	27.0 (8.9)	30.0^{a} (24.2–37.3)	3.1^{b} (2.0–4.6)
σ_B (Porcelain surface)		($p < 0.001$)	($p < 0.001$)
VM 9 (9.1:9.0–9.2)	154.1 (10.3)	158.9^{ac} (153.0–164.4)	18.3^{a} (11.3–29.7)
CCK (9.2)	129.8 (20.6)	137.2^{b} (128.5–146.4)	9.8^{ab} (5.8–16.6)
Experimental (8.45)	128.6 (20.7)	137.1^{ab} (124.4–151.2)	6.7^{ab} (4.3–11.5)
Experimental (9.04)	158.1 (18.7)	166.3^{c} (154.7–178.8)	9.1^{ab} (5.8–14.4)
Experimental (9.61)	171.1 (40.1)	186.8^{c} (159.2–219.1)	4.1^{b} (2.7–6.3)

CTE: coefficient of thermal expansions, BFS: biaxial flexural strength, σ_T, σ_B: biaxial stresses at the top and bottom surfaces of the specimen, respectively. σ_1, σ_2: the biaxial flexural strengths at the interface in the bottom and top layers, respectively. VM9: VITA VM 9, CCK: Cercon Ceram Kiss, Experimental: Vintage ZR. Different lowercase letters within each parameter indicate significant differences among the groups ($p < 0.05$).
[1] indicates the compressive stress.

face of the porcelain layer (σ_1) and a small thermal gradient between the outer and inner surface of the porcelain layer (Table 3). Some researchers have indicated that slight residual compressive stresses (−20 or −25 MPa) are beneficial for porcelain-zirconia interfacial adhesion [9,20]. Moreover, Wang et al. [45] reported that the residual compressive stresses in the core layer had a slight beneficial effect on the strengths of bilayered porcelain-Y-TZP specimens due to the small thermal gradients between the outer and inner surfaces of the porcelain layer. However, it should be noted that thermal characteristics of the porcelain-zirconia specimen might have been related not only to the CTE mismatch between materials, but also to other factors (*e.g.* the firing schedule, thermo-elastic properties and thicknesses of structures, and the chemical composition and T_g of the porcelain material). Our results also confirmed that the VM9 and experimental (CTE: 9.04 ppm/°C) groups showed higher thermal stresses than the CCK group even though they had similar CTE values. These differences might have been related to the chemical composition of the porcelain material; porcelain materials in this study had different chemical compositions including different ratios of leucite [46–48]. One possible explanation is that the existence of leucite crystals could be related to the structural relaxation of porcelain that generated lower magnitude transient and residual stresses during cooling due to its viscosity increase and flow reduction during firing [37].

Furthermore, Swain [49] stated that residual stresses may arise from a CTE mismatch and from tempering associated with fast-cooling. Fast-cooling causes high transient thermal gradients, resulting in excessive tempering tensile stresses within the porcelain layer, and high tempering/compressive residual stresses on the surface due to poor thermal conductivity and diffusivity of materials such as porcelain and zirconia [31,42,43]. Benetti et al. [50] observed remarkable temperature gradients for a fast-cooled Y-TZP-based crown, indicating that slow-cooling was important for preventing high-magnitude thermal gradients. Even though the slow-cooling protocol was used here, CTE mismatches also affected stress distribution. This was supported by a previous study showing that slow-cooling reduced temperature gradients and residual stresses within the porcelain layer, but that temperature differences up to 88 °C were observed between the outer and inner surfaces of the porcelain layer [44].

Unfortunately, it is still unclear how the cooling protocol influences thermal stresses because the cooling rate and

Table 6 – Number of the fracture fragments of the Ce-TZP/A substrate.

Porcelain material (CTE; ppm/°C)	Two pieces	Three pieces	p
VM 9 (9.1:9.0–9.2)	6	4	
CCK (9.2)	8	2	
Experimental (8.45)	9	1	0.016
Experimental (9.04)	5	5	
Experimental (9.61)	2	8	

VM9: VITA VM 9, CCK: Cercon Ceram Kiss, Experimental: Vintage ZR.

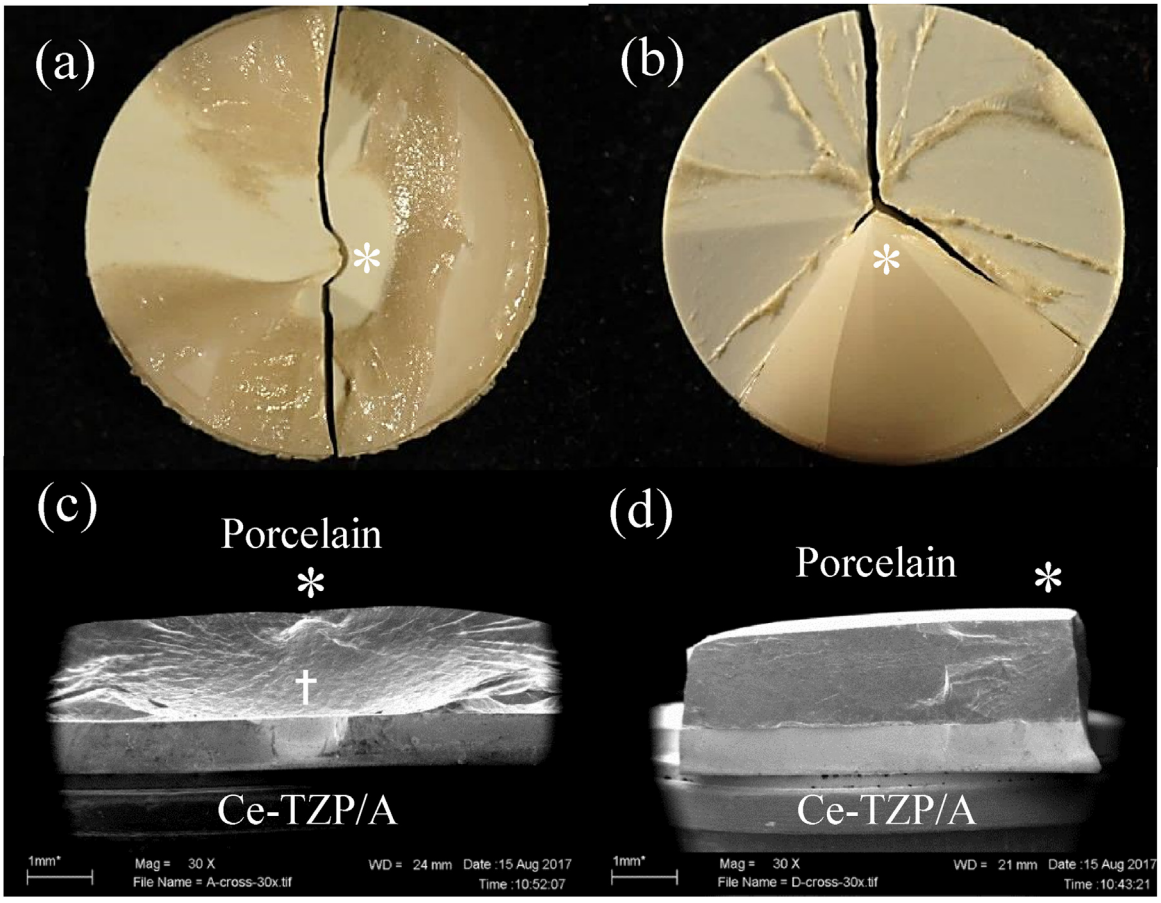

Fig. 3 – Micrographs (magnification: 10×; a,b) and SEM cross-sectional images (magnification: 30×; c,d) of the fractured specimens. a,c; the Ce-TZP/A specimen is shown with two fractured pieces (experimental porcelain with a CTE of 9.04 ppm/°C), b,d: the Ce-TZP/A specimen is shown with three fractured pieces (experimental porcelain with a CTE of 9.61 ppm/°C), respectively. * and † indicate the fracture origin of the specimens and the defect of the Ce-TZP/A layer at the interface, respectively.

possible stress relaxation by non-elastic deformation at temperatures below T_g were not considered for the calculated thermal stresses. These stresses were dependent on parameters such as CTE mismatch, layer thickness, elastic modulus, and T_g, and showed different stress gradients and discontinuous stresses in the disks (Eqs. (1)–(4)). Consequently, our results of biaxial thermal and flexural testing should be considered separately whereas Hsueh et al. conducted combined thermal stresses/ring-on-ring tests for bilayered disks using the same closed-form solutions as in this study [36]. In addition, no appropriate solution is available for piston-on-three-ball tests. Therefore, further study is needed to construct an adequate analytical model.

4.2. *Biaxial flexural test*

4.2.1. *Testing method used in this study*

High-strength ceramics are required to withstand excessive tensile stresses that develop on the bridge connector in posterior FPDs during mastication [51]. The mechanical properties of porcelain and zirconia, and their bond strengths should be evaluated for clinical use as the survival times of bilayered restorations are strongly dependent on these factors [53,54]. The biaxial flexural strength test is a more useful method than uniaxial flexural tests as dental materials are subjected to multiaxial loading in clinical situations [55]; however, this has only been defined for monolithic materials in ISO 6872:2008 [38]. Thus, biaxial flexural strengths were calculated here using recent closed-form solutions derived by Hsueh et al. and Hsueh and Kelly [32,33]. This approach was able to calculate strengths at the interface of the layers and the external surfaces of the bilayered disks, identified the stress distributions through the entire thickness, and determined the location of the maximum tensile stress that occurred at the interface or in the bottom surface of the disk. Additionally, these results are consistent with those of finite element analyses (FEA) and flexural strengths calculated by the Roark's formula (for bimetallic circular plates) at the top and bottom surfaces of the specimen.

4.2.2. *Calculated biaxial flexural strengths*

Compressive stresses generally occur at the top surface of the monolithic ceramic in the biaxial flexural test while tensile stresses occur at the bottom surface. For evaluating ceramic strength, only the maximum tension is required as compres-

sive stress is less critical [17,33]. However, predicting stress distribution is more complicated for bilayered ceramics.

Although the biaxial flexural strengths calculated here indicated that tensile stresses occurred in the entire porcelain layer, compressive stresses in the surface of the Ce-TZP/A layer shifted to tensile stresses at the interface of the specimens (Fig. 2b). Regarding tensile stresses, σ_1 calculated using the Hsueh et al. formulas and σ_B calculated using the Hsueh and Kelly formulas showed a similar trend, indicating that these results were the appropriate relationship for the calculation of stresses between different layers of the specimens. In most specimens with higher CTE porcelains, higher Weibull characteristic strengths were observed at both internal (σ_1 and σ_2) and external (σ_T and σ_B) surfaces of each layer. These strengths were dependent on the residual thermal stress as stated above, and smaller CTE mismatches between the materials showed lower residual stresses resulting in higher strengths. Exceptionally, the VM9 and experimental porcelain with a CTE of 9.04 ppm/°C showed higher stresses than the CCK group, even though they had similar CTE values. For the biaxial flexural test, the strengths may also be influenced by the porcelain type and layer thickness. For instance, Lin et al. [56] reported that monolithic leucite-reinforced glass-ceramic showed lower flexural strength than monolithic lithium-disilicate glass-ceramic. In contrast, Meirelles et al. [37] reported that bilayered porcelain-Y-TZP disks (both for porcelain with and without leucite) showed similar flexural strengths even if a CTE difference was observed between the porcelain materials (9.1 and 9.4 ppm/°C).

In such cases, the authors clarified that when using a 1.0 mm thick porcelain layer, the magnitudes of the stresses generated both by the difference in thermal contraction and changes in cooling rate were not sensitive in the bilayered specimens. Thus, these conflicting results might also be associated with the core-to-porcelain thickness ratio of the specimens, and the cooling protocol. In the case of thin porcelain, these factors probably have negligible effects.

4.2.3. *Fracture mode and origin*

Two different peaks of tensile stress were observed at the interface of the Ce-TZP/A layer (σ_2) and at the surface of the porcelain layer (σ_B: the bottom surface of the specimen) (Fig. 2b). Our results were consistent with previous reports using FEA which showed a peak compressive stress underneath the loading piston and two different peaks of tensile stresses at the interface and bottom surface of the specimen when the tension side was the porcelain layer [25,36,57,58]. These peaks depended on the core-to-porcelain thickness ratio, mechanical properties of the materials, and the testing method. In addition, the elastic constants and thicknesses of the constituent layers influenced the location of the maximum tension in a bilayered disk [52]. In our cases using the Hsueh and Kelly formula (Eqs. (10)–(14)), due to the same core-to-porcelain thickness ratio and the porcelain layer thickness being used, the strengths were sensitive to elastic modulus, thickness, and Poisson's ratio of the respective layer, showing that the location of the maximum tensile stress was observed at σ_B.

The difference in these factors implicated the fracture mode and origin. According to a previous study, cracks could originate from any tensile layer, or at the interface between the layers of a bilayered specimen when the porcelain layer was the bottom surface [32]. Here, the crack always originated from the bottom surface of the specimen due to the brittle porcelain material. The differences between σ_B and σ_1 were high in the specimens with higher CTE porcelain, resulting in higher stress gradients in the porcelain layer (Table 5). These stress gradients were expected to have caused the Ce-TZP/A to fracture into three pieces. Our results were consistent with a previous study [59] in which a positive correlation was found between fracture stress and the fractured pieces of monolithic ceramic specimens in biaxial flexural tests; higher fracture stress resulted in a larger number of fractured pieces. Thus, three fracture pieces of Ce-TZP/A were observed in the specimens with a smaller CTE mismatch, which showed higher strength and continuous crack propagation. In contrast, the specimens with a higher CTE mismatch resulted in the Ce-TZP/A fracturing into two pieces. A semicircular defect also developed at the interface because the strengths were lower than those with a lower CTE mismatch, resulting in slow stress gradients and crack propagation in the porcelain layer.

4.2.4. *Influence of the cooling protocol*

To clarify the influence of the cooling protocol as observed in previous research [25], a comparison of biaxial flexural strengths was made for specimens subjected to fast- and slow-cooling.

The Weibull characteristic strength (σ_0) and modulus (m) of biaxial flexural strengths of the specimens (core-to-porcelain thickness: 0.8 mm/1.5 mm) depended on the CTE mismatch and porcelain type (Fig. A2). Although fast-cooling did not influence the strengths in the bottom surface of the specimens (σ_B) [25], slow-cooling predominantly resulted in lower strengths in the case of the lower CTE porcelain. Our results were consistent with a previous study [60] indicating that fast-cooling caused residual compressive stress within the porcelain layer, which increased the strength of the bilayered specimen. In addition, slow-cooling enhanced the resistance to porcelain chipping of Y-TZP-based crowns that were prepared using porcelain with larger a CTE mismatch (VM9; +1.4 ppm/°C) while none of the cooling rates influenced the crowns that used porcelain with a CTE close to the core material (Lava Ceram; +0.3 ppm/°C) [29]. Consequently, slow-cooling could change the viscosity or crystallization behavior of the porcelain, and may affect the strengths and enhanc the reliability of bilayered crowns when porcelain with a large CTE mismatch was used. However, attention must be paid to the cooling protocol when comparing strength results because Almeida et al. [31] pointed out that the cooling protocol is not well defined, so many different cooling methods have been presented in previous studies. Here, the firing schedule of the dental furnace was also adjusted according to the manufacturer's instructions.

Finally, the data obtained here could not be directly compared to clinical situations because the Ce-TZP/A framework had a specific form and its thickness was not homogeneous

and constant. Further study is needed to clarify the adequate combination of Ce-TZP/A substrate and porcelain layer thickness required when using the actual geometry of a single crown and FPD in clinical use.

Conclusion

Within the limitations of this study, the biaxial flexural strengths and stress distributions at both external and internal surfaces of slow-cooled bilayered porcelain-Ce-TZP/A disks were influenced by porcelain materials. Smaller CTE mismatches between the materials were preferable.

Author contributions

T. S. contributed to conception, design, data analysis, interpretation and wrote the paper; J. G-G. contributed to conception, design, data interpretation and critical revision of the manuscript; V.W. S.S. C.S. and E.S. contributed to specimen preparation and data acquisition, analysis, and critical revision of the manuscript. All co-authors gave their final approval.

Acknowledgments

The authors are grateful to Panasonic Healthcare (Japan), VITA Zahnfabrik (Germany), Degudent GmbH (Germany) and Shofu (Japan) for providing the materials. The authors are also grateful to Dekema Dental-Keramiköfen (Germany) and Wieland Dental + Technik GmbH (Pforzheim, Germany) for supporting the dental furnace and CTE measurements.

Appendix A

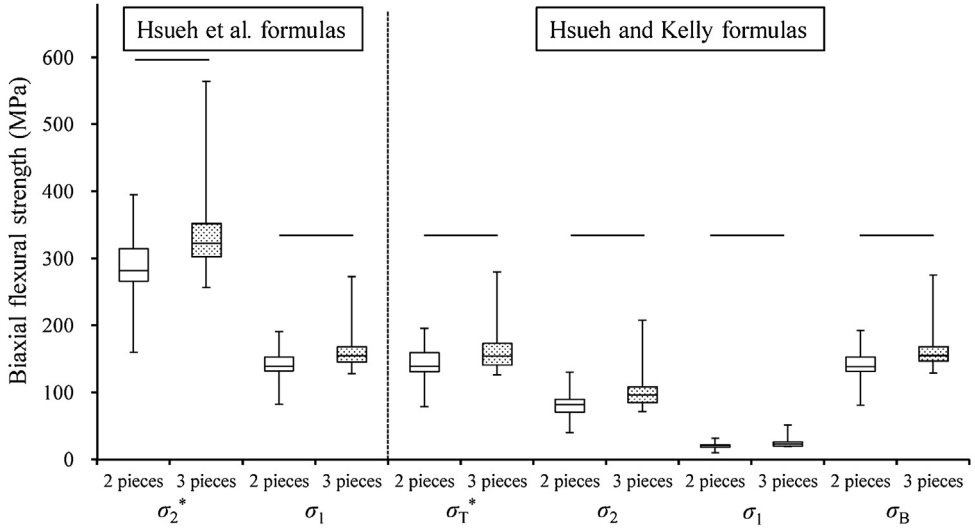

Fig. A1 – Comparisons of biaxial flexural strengths (median) for the Ce-TZP/A specimens fractured into two and three pieces. * indicates the compressive stress. The horizontal bars indicate significant differences between the specimens (Mann–Whitney U test, $p < 0.05$).

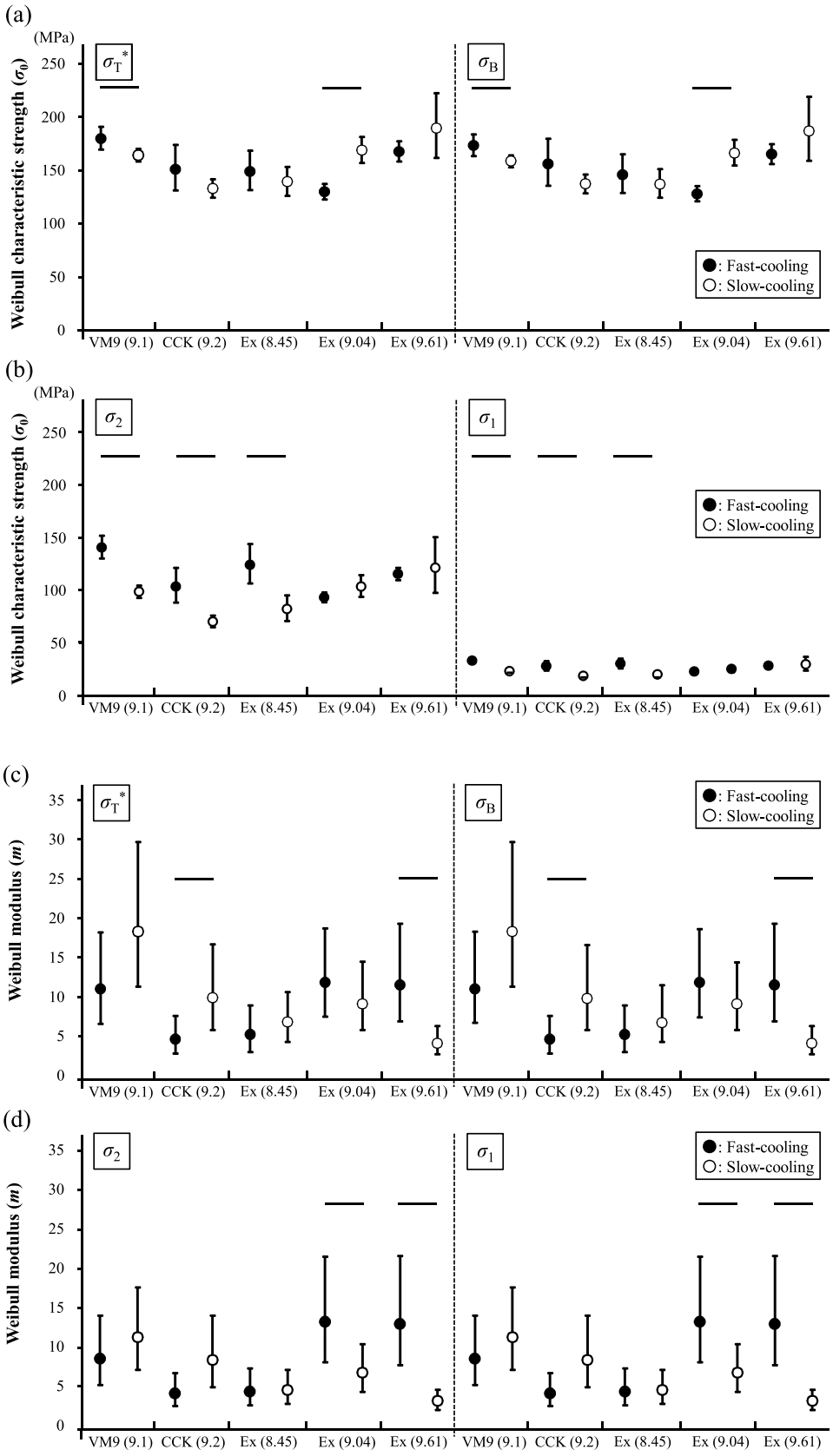

Fig. A2 – Comparisons of Weibull characteristic strength (σ_0; a,b) and modulus (m; c,d) for biaxial flexural stresses subjected to piston-on-three-ball tests in the specimens between fast- and slow-cooling protocols (core-to-porcelain thickness; 0.8 mm/1.5 mm). VM9: VITA VM 9, CCK; Cercon Ceram Kiss, Ex; Experimental porcelain: Vintage ZR (CTE: ppm/°C). Fast-cooling data were previously reported by Sawada et al. [25].

REFERENCES

[1] Dündar M, Ozcan M, Gökçe B, Cömlekoğlu E, Leite F, Valandro LF. Comparison of two bond strength testing methodologies for bilayered all-ceramics. Dent Mater 2007;23:630–6, http://dx.doi.org/10.1016/j.dental.2006.05.004.

[2] Tanaka K, Tamura J, Kawanabe K, Nawa M, Uchida M, Kokubo T, et al. Phase stability after aging and its influence on pin-on-disk wear properties of Ce-TZP/Al_2O_3 nanocomposite and conventional Y-TZP. J Biomed Mater Res A 2003;67:200–7, http://dx.doi.org/10.1002/jbm.a.10006.

[3] Ban S, Sato H, Suehiro Y, Nakanishi H, Nawa M. Biaxial flexure strength and low temperature degradation of Ce-TZP/Al_2O_3 nanocomposite and Y-TZP as dental restoratives. J Biomed Mater Res B Appl Biomater 2008;87:492–8, http://dx.doi.org/10.1002/jbm.b.31131.

[4] Zarone F, Russo S, Sorrentino R. From porcelain-fused-to-metal to zirconia: clinical and experimental considerations. Dent Mater 2011;27:83–96, http://dx.doi.org/10.1016/j.dental.2010.10.024.

[5] Miyazaki T, Nakamura T, Matsumura H, Ban S, Kobayashi T. Current status of zirconia restoration. J Prosthodont Res 2013;57:236–61, http://dx.doi.org/10.1016/j.jpor.2013.09.001.

[6] Omori S, Komada W, Yoshida K, Miura H. Effect of thickness of zirconia-ceramic crown frameworks on strength and fracture pattern. Dent Mater J 2013;32:189–94, http://dx.doi.org/10.4012/dmj.2012-255.

[7] Ban S. Reliability and properties of core materials for all-ceramic dental restorations. Jpn Dent Sci Rev 2008;44:3–21, http://dx.doi.org/10.1016/j.jdsr.2008.04.001.

[8] Shiraishi T, Watanabe I. Thickness dependence of light transmittance, translucency and opalescence of a ceria-stabilized zirconia/alumina nanocomposite for dental applications. Dent Mater 2016;32:660–7, http://dx.doi.org/10.1016/j.dental.2016.02.004.

[9] Freifrau Von Maltzahn N, Kleibe M, Stiesch M, Hübsch C, Kohorst P. Interfacial adhesion of zirconia/veneer bilayers with different thermal characteristics. Dent Mater J 2014;33:583–90, http://dx.doi.org/10.4012/dmj.2013-181.

[10] Aboushelib MN, de Jager N, Kleverlaan CJ, Feilzer AJ. Microtensile bond strength of different components of core veneered all-ceramic restorations. Dent Mater 2005;21:984–91, http://dx.doi.org/10.1016/j.dental.2005.03.013.

[11] Pjetursson BE, Sailer I, Makarov NA, Zwahlen M, Thoma DS. All-ceramic or metal-ceramic tooth-supported fixed dental prostheses (FDPs)? A systematic review of the survival and complication rates. Part II: multiple-unit FDPs. Dent Mater 2015;31:624–39, http://dx.doi.org/10.1016/j.dental.2015.02.013.

[12] Pjetursson BE, Sailer I, Makarov NA, Zwahlen M, Thoma DS. Corrigendum to "All-ceramic or metal-ceramic tooth-supported fixed dental prostheses (FDPs)? A systematic review of the survival and complication rates. Part II: Multiple-unit FDPs" [Dental Materials 31(6)(2015)624-639]. Dent Mater 2017;33:e48–51, http://dx.doi.org/10.1016/j.dental.2016.09.033.

[13] Sailer I, Balmer M, Hüsler J, Hämmerle CHF, Känel S, Thoma DS. Comparison of fixed dental prostheses with zirconia and metal frameworks: five-year results of a randomized controlled clinical trial. Int J Prosthodont 2017;30(5):426–8, http://dx.doi.org/10.11607/ijp.5183.

[14] Philipp A, Fischer J, Hämmerle CH, Sailer I. Novel ceria-stabilized tetragonal zirconia/alumina nanocomposite as framework material for posterior fixed dental prostheses: preliminary results of a prospective case series at 1 year of function. Quintessence Int 2010;41:313–9, http://dx.doi.org/10.5167/uzh-33839.

[15] Tanaka S, Takaba M, Ishiura Y, Kamimura E, Baba K. A 3-year follow-up of ceria-stabilized zirconia/alumina nanocomposite (Ce-TZP/A) frameworks for fixed dental prostheses. J Prosthodont Res 2015;59:55–61, http://dx.doi.org/10.1016/j.jpor.2014.11.006.

[16] Huettig F, Keitel JP, Prutscher A, Spintzyk S, Klink A. Fixed dental prostheses and single-tooth crowns based on Ceria-stabilized tetragonal zirconia/alumina nanocomposite frameworks: outcome after 2 years in a clinical trial. Int J Prosthodont 2017;30:461–4, http://dx.doi.org/10.11607/ijp.5116.

[17] Fischer J, Stawarczyk B, Tomic M, Strub JR, Hämmerle CH. Effect of thermal misfit between different veneering ceramics and zirconia frameworks on in vitro fracture load of single crowns. Dent Mater J 2007;26:766–72, http://dx.doi.org/10.4012/dmj.26.766.

[18] Fischer J, Stawarczyk B. Compatibility of machined Ce-TZP/Al_2O_3 nanocomposite and a veneering ceramic. Dent Mater 2007;23:1500–5, http://dx.doi.org/10.1016/j.dental.2007.01.005.

[19] Benetti P, Kelly JR, Sanchez M, Della Bona A. Influence of thermal gradients on stress state of veneered restorations. Dent Mater 2014;30:554–63, http://dx.doi.org/10.1016/j.dental.2014.02.020.

[20] Göstemeyer G, Jendras M, Borchers L, Bach FW, Stiesch M, Kohorst P. Effect of thermal expansion mismatch on the Y-TZP/veneer interfacial adhesion determined by strain energy release rate. J Prosthodont Res 2012;56:93–101, http://dx.doi.org/10.1016/j.jpor.2011.09.002.

[21] Ban S, Nawa M, Sugata F, Tsuruki J, Kono H, Kawai T. HRTEM observation of bonding interface between Ce-TZP/Al_2O_3 nanocomposite and porcelain. Dent Mater J 2014;33:565–9, http://dx.doi.org/10.4012/dmj.2014-035.

[22] Aboushelib MN, Wang H. Influence of crystal structure on debonding failure of zirconia veneered restorations. Dent Mater 2013;29:e97–102, http://dx.doi.org/10.1016/j.dental.2013.04.008.

[23] Fischer J, Stawarczyk B, Trottmann A, Hämmerle CH. Impact of thermal properties of veneering ceramics on the fracture load of layered Ce-TZP/A nanocomposite frameworks. Dent Mater 2009;25:326–30, http://dx.doi.org/10.1016/j.dental.2008.08.001.

[24] Terui Y, Sato K, Goto D, Hotta Y, Tamaki Y, Miyazaki T. Compatibility of Ce-TZP/Al_2O_3 nanocomposite frameworks and veneering porcelains. Dent Mater J 2013;32:839–46, http://dx.doi.org/10.4012/dmj. 2012-039.

[25] Sawada T, Schille C, Wagner V, Spintzyk S, Schweizer E, Geis-Gerstorfer J. Biaxial flexural strength on the bilayered disk composed of ceria-stabilized zirconia/alumina nanocomposite (Ce-TZP/A) and veneering porcelain. Dent Mater 2018;34:1199–210, http://dx.doi.org/10.1016/j.dental.2018.05.003.

[26] Aboushelib MN, Kleverlaan CJ, Feilzer AJ. Microtensile bond strength of different components of core veneered all-ceramic restorations. Part II: zirconia veneering ceramics. Dent Mater 2006;22:857–63, http://dx.doi.org/10.1016/j.dental.2005.11.014.

[27] de Kler M, de Jager N, Meegdes M, van der Zel JM. Influence of thermal expansion mismatch and fatigue loading on phase changes in porcelain veneered Y-TZP zirconia discs. J Oral Rehabil 2007;34:841–7, http://dx.doi.org/10.1111/j.1365-2842.2006.01675.x.

[28] Alayad AS. Effect of zirconia core thickness and veneer firing cycle on the biaxial flexural strength of veneering ceramic. J Prosthodont 2018, http://dx.doi.org/10.1111/jopr.12929 [in press].

[29] Belli R, Frankenberger R, Appelt A, Schmitt J, Baratieri LN, Greil P, et al. Thermal-induced residual stresses affect the

lifetime of zirconia-veneer crowns. Dent Mater 2013;29:181–90, http://dx.doi.org/10.1016/j.dental.2012.11.015.
[30] Guazzato M, Walton TR, Franklin W, Davis G, Bohl C, Klineberg I. Influence of thickness and cooling rate on development of spontaneous cracks in porcelain/zirconia structures. Aust Dent J 2010;55:306–10, http://dx.doi.org/10.1111/j.1834-7819.2010.01239.x.
[31] Almeida Jr AA, Longhini D, Domingues NB, Santos C, Adabo GL. Effects of extreme cooling methods on mechanical properties and shear bond strength of bilayered porcelain/3Y-TZP specimens. J Dent 2013;41:356–62, http://dx.doi.org/10.1016/j.jdent.2013.01.005.
[32] Hsueh CH, Luttrell CR, Becher PF. Analyses of multilayered dental ceramics subjected to biaxial flexure tests. Dent Mater 2006;22:460–9, http://dx.doi.org/10.1016/j.dental.2005.04.037.
[33] Hsueh CH, Kelly JR. Simple solutions of multilayered discs subjected to biaxial moment loading. Dent Mater 2009;25:506–13, http://dx.doi.org/10.1016/j.dental.2008.10.002.
[34] Huang CW, Hsueh CH. Piston-on-three-ball versus piston-on-ring in evaluating the biaxial strength of dental ceramics. Dent Mater 2011;27:e117–23, http://dx.doi.org/10.1016/j.dental.2011.02.011.
[35] Hsueh CH. Modeling of elastic deformation of multilayers due to residual stresses and eternal bending. J Appl Phys 2002;91:9652–6, http://dx.doi.org/10.1063/1.1478137.
[36] Hsueh CH, Thompson GA, Jadaan OM, Wereszczak AA, Becher PF. Analyses of layer-thickness effects in bilayered dental ceramics subjected to thermal stresses and ring-on-ring tests. Dent Mater 2008;24:9–17, http://dx.doi.org/10.1016/j.dental.2006.12.009.
[37] Meirelles PD, Spigolon YO, Borba M, Benetti P. Leucite and cooling rate effect on porcelain-zirconia mechanical behavior. Dent Mater 2016;32:e382–388, http://dx.doi.org/10.1016/j.dental.2016.09.018.
[38] International Organization for Standardization. ISO 6872:2008. Dentistry-ceramic materials. Geneva, Switzerland: International Organization for Standardization; 2008.
[39] El-Korashy DI, El-Refai DA. Mechanical properties and bonding potential of partially stabilized zirconia treated with different chemomechanical treatments. J Adhes Dent 2014;16:365–76, http://dx.doi.org/10.3290/j.jad.a32069.
[40] Quinn JB, Quinn GD. A practical and systematic review of Weibull statistics for reporting strengths of dental materials. Dent Mater 2010;26:135–47, http://dx.doi.org/10.1016/j.dental.2009.09.006.
[41] Bütikofer L, Stawarczyk B, Roos M. Two regression methods for estimation of a two-parameter Weibull distribution for reliability of dental materials. Dent Mater 2015;31:e33–50, http://dx.doi.org/10.1016/j.dental.2014.11.014.
[42] Göstemeyer G, Jendras M, Dittmer MP, Bach FW, Stiesch M, Kohorst P. Influence of cooling rate on zirconia/veneer interfacial adhesion. Acta Biomater 2010;6:4532–8, http://dx.doi.org/10.1016/j.actbio.2010.06.026.
[43] Mainjot AK, Najjar A, Jakubowicz-Kohen BD, Sadoun MJ. Influence of thermal expansion mismatch on residual stress profile in veneering ceramic layered on zirconia: measurement by hole-drilling. Dent Mater 2015;31:1142–9, http://dx.doi.org/10.1016/j.dental.2015.06.017.
[44] Tholey MJ, Swain MV, Thiel N. Thermal gradients and residual stresses in veneered Y-TZP frameworks. Dent Mater 2011;27:1102–10, http://dx.doi.org/10.1016/j.dental.2011.08.001.
[45] Wang G, Zhang S, Bian C, Kong H. Effect of thickness ratio on load-bearing capacity of bilayered dental ceramics. J Prosthodont 2015;24:17–24, http://dx.doi.org/10.1111/jopr.12169.
[46] Choi BK, Han JS, Yang JH, Lee JB, Kim SH. Shear bond strength of veneering porcelain to zirconia and metal cores. J Adv Prosthodont 2009;1:129–35, http://dx.doi.org/10.4047/jap.2009.1.3.129.
[47] Luo H, Tang X, Dong Z, Tang H, Nakamura T, Yatani H. The influences of accelerated aging on mechanical properties of veneering ceramics used for zirconia restorations. Dent Mater J 2016;35:187–93, http://dx.doi.org/10.4012/dmj.2015-115.
[48] Longhini D, Rocha CO, Medeiros IS, Fonseca RG, Adabo GL. Effect of glaze cooling rate on mechanical properties of conventional and pressed porcelain on zirconia. Braz Dent J 2016;27:524–31, http://dx.doi.org/10.1590/0103-6440201600709.
[49] Swain MV. Unstable cracking (chipping) of veneering porcelain on all-ceramic dental crowns and fixed partial dentures. Acta Biomater 2009;5:1668–77, http://dx.doi.org/10.1016/j.actbio.2008.12.016.
[50] Benetti P, Kelly JR, Della Bona A. Analysis of thermal distributions in veneered zirconia and metal restorations during firing. Dent Mater 2013;29:1166–72, http://dx.doi.org/10.1016/j.dental.2013.08.212.
[51] Studart AR, Filser F, Kocher P, Lüthy H, Gauckler LJ. Mechanical and fracture behavior of veneer-framework composites for all-ceramic dental bridges. Dent Mater 2007;23:115–23, http://dx.doi.org/10.1016/j.dental.2005.12.009.
[52] Yilmaz H, Nemli SK, Aydin C, Bal BT, Tıraş T. Effect of fatigue on biaxial flexural strength of bilayered porcelain/zirconia (Y-TZP) dental ceramics. Dent Mater 2011;27:786–95, http://dx.doi.org/10.1016/j.dental.2011.03.019.
[53] Fischer J, Grohmann P, Stawarczyk B. Effect of zirconia surface treatments on the shear strength of zirconia/veneering ceramic composites. Dent Mater J 2008;27:448–54, http://dx.doi.org/10.4012/dmj.27.448.
[54] Schatz C, Strickstrock M, Roos M, Edelhoff D, Eichberger M, Zylla IM, et al. Influence of specimens preparation and test methods on the flexural strength results of monolithic zirconia materials. Materials 2016;9:180, http://dx.doi.org/10.3390/ma9030180.
[55] Sinmazisik G, Tarcin B, Demirbas B, Gulmez T, Bor E, Ozer F. The effect of zirconia thickness on the biaxial flexural strength of zirconia ceramic bilayered discs. Dent Mater J 2015;34:640–7, http://dx.doi.org/10.4012/dmj.2014-340.
[56] Lin WS, Ercoli C, Feng C, Morton D. The effect of core material, veneering porcelain, and fabrication technique on the biaxial flexural strength and weibull analysis of selected dental ceramics. J Prosthodont 2012;21:353–62, http://dx.doi.org/10.1111/j.1532-849X.2012.00845.x.
[57] Guazzato M, Proos K, Quach L, Swain MV. Strength, reliability and mode of fracture of bilayered porclain/zirconia (Y-TZP) dental ceramics. Biomaterials 2004;25:5045–52, http://dx.doi.org/10.1016/j.biomaterials.2004.02.036.
[58] Guazzato M, Proos K, Sara G, Swain MV. Strength, reliability, and mode of fracture of bilayered porcelain/core ceramics. Int J Prosthodont 2004;17:142–9.
[59] Gonzaga CC, Cesar PF, Miranda Jr WG, Yoshimura HN. Slow crack growth and reliability of dental ceramics. Dent Mater 2011;27:394–406, http://dx.doi.org/10.1016/j.dental.2010.10.025.
[60] Taskonak B, Borges GA, Mecholsky Jr JJ, Anusavice KJ, Moore BK, Yan J. The effects of viscoelastic parameters on residual stress development in a zirconia/glass bilayer dental ceramic. Dent Mater 2008;24:1149–55, http://dx.doi.org/10.1016/j.dental.2008.01.004.